

pubs.acs.org/jcim Article

The Effects of N-Linked Glycosylation on SLC6 Transporters

Matthew C. Chan and Diwakar Shukla*



Cite This: https://doi.org/10.1021/acs.jcim.2c00940



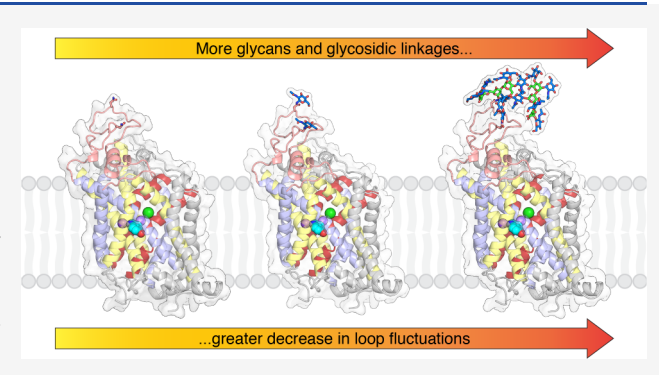
ACCESS

Metrics & More

Article Recommendations

Supporting Information

ABSTRACT: Membrane transporters of the solute carrier 6 (SLC6) family mediate various physiological processes by facilitating the translocation of amino acids, neurotransmitters, and other metabolites. In the body, the activity of these transporters is tightly controlled through various post-translational modifications with implications on protein expression, stability, membrane trafficking, and dynamics. While N-linked glycosylation is a universal regulatory mechanism among eukaryotes, a consistent mechanism of how glycosylation affects the SLC6 transporter family remains elusive. It is generally believed that glycans influence transporter stability and membrane trafficking; however, the role of glycosylation on transporter dynamics remains disputable, with differing conclusions among individual transporters across the SLC6



family. In this study, we collected over 1 ms of aggregated all-atom molecular dynamics (MD) simulation data to systematically identify the impact of N-glycans on SLC6 transporter dynamics. We modeled four human SLC6 transporters, the serotonin, dopamine, glycine, and B⁰AT1 transporters, by first simulating all possible combinations of a glycan attached to each glycosylation site followed by investigating the effect of larger, oligo-N-linked glycans to each transporter. The simulations reveal that glycosylation does not significantly affect the transporter structure but alters the dynamics of the glycosylated extracellular loop and surrounding regions. The structural consequences of glycosylation on the loop dynamics are further emphasized with larger glycan molecules attached. However, no apparent differences in ligand stability or movement of the gating helices were observed, and as such, the simulations suggest that glycosylation does not have a profound effect on conformational dynamics associated with substrate transport.

■ INTRODUCTION

The solute carrier 6 (SLC6) family is a class of secondary active cotransporters that mediates the reuptake of amino acids, biogenic amines, osmolytes, and metabolites, thereby maintaining cellular homeostasis throughout the body. These transporters harness the energy of a favorable sodium ion concentration gradient to power the uphill transport of substrates across the plasma membrane. Many SLC6 transporters are also members of the neurotransmitter:sodium symporter (NSS) family and are essential for regulating neurotransmission in the central and peripheral nervous systems. Description of the secondary across the plasma are essential for regulating neurotransmission in the central and peripheral nervous systems.

Members of the SLC6 family adopt the canonical 12 transmembrane (TM) helix LeuT fold with the transporter core formed by helices 1–5 and 6–10 arranged in a 5 + 5 inverted pseudosymmetric repeat topology and two additional helices, 11 and 12, residing on the periphery of the core (Figure 1A).³ The transport of substrates is dictated by the structural rearrangements that enable the transporter to alternate between an extracellular accessible or outward-facing (OF) conformation to the intracellular accessible or inward-facing (IF) conformation. Specifically, SLC6 transporters undergo a rocking-bundle mechanism in which the trans-

membrane helices 1 and 6 serve as gating helices that undergo a "rocking" conformational shift from the rigid scaffold domain, thus enabling the opening and closure of the orthosteric binding site. The recent determination of various SLC6 transporters and its bacterial homologues have established the structural basis of substrate and inhibitor molecule binding. The serve as a service of the orthogonal structural basis of substrate and inhibitor molecule binding.

Despite sharing 20–25% sequence identity with human SLC6 transporters, prokaryotic SLC6 proteins have historically illuminated the elusive structure—function relationships of this important class of transporters. While the general understanding of transport and conformational dynamics may be applied to characterize human transporters, the effects of post-translational modifications cannot be inferred as prokaryotic homologues do not share the similar mechanisms or structural features of regulatory components as do their

Received: July 24, 2022



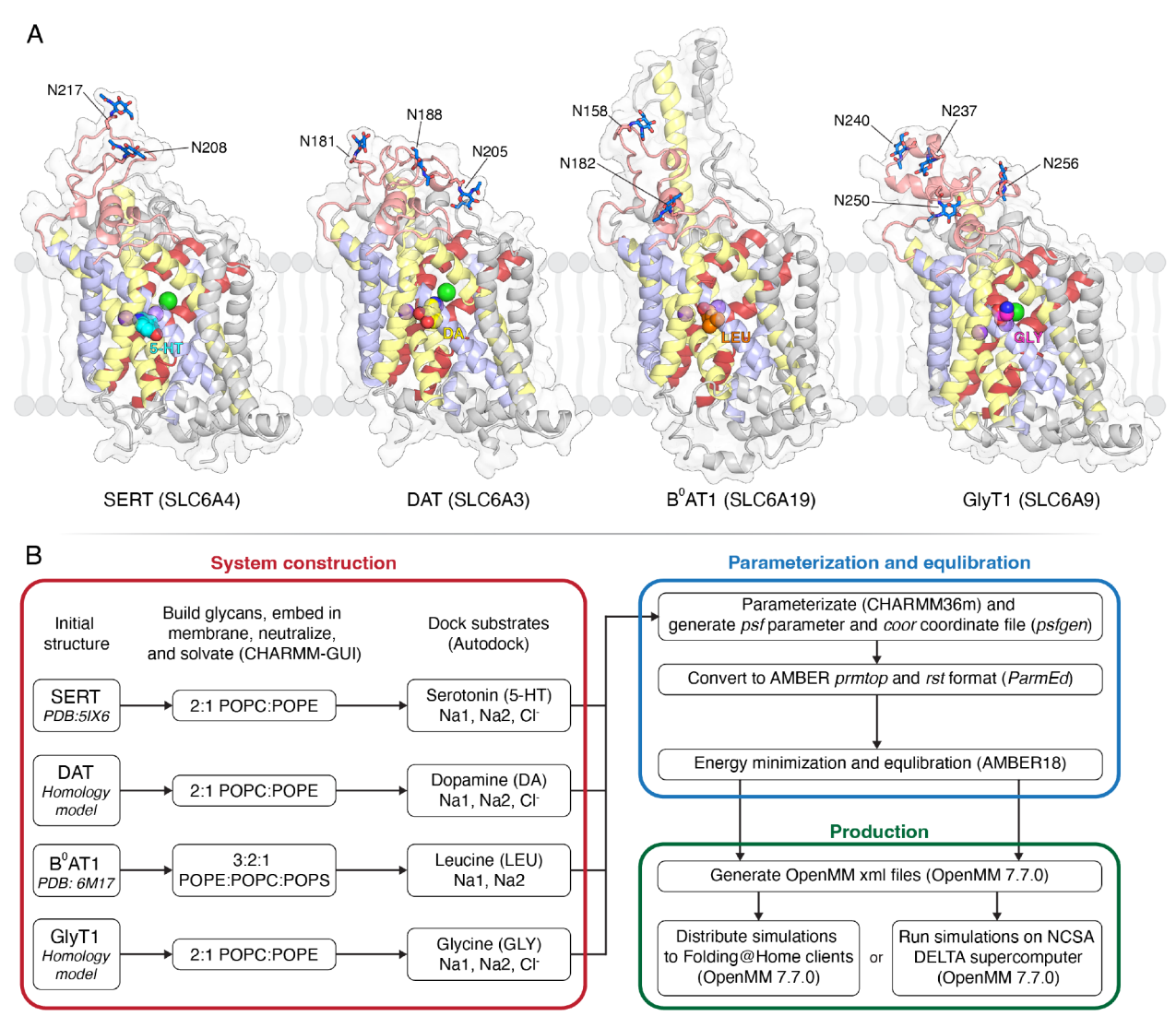


Figure 1. Simulation overview of the conducted study. (A) Starting structures of SLC6 transporters used for MD simulations. Transporters were modeled in the outward-facing conformation with substrates and ions initial bound in the orthosteric pocket. Sodium and chloride ions are shown as purple and green spheres, respectively. Respective substrates are shown as spheres (5-HT: serotonin, DA: dopamine, LEU: leucine, GLY: glycine). The transporters are shown in cartoon representation and colored as follows: gating helices 1 and 6, red; 5 + 5 helix repeats, yellow and pale blue; extracellular loop 2, salmon. N-linked glycosylation sites with an N-acetylglucosamine glycan are represented as sticks and labeled accordingly. (B) Simulation workflow for the four studied SLC6 transporters. Simulations were parametrized using the CHARMM36m force field. Energy minimization and equilibration simulations were performed using AMBER18. The subsequent simulation output files were converted to OpenMM xml files for production simulations either on a Folding@Home distributive computing platform or the NCSA DELTA supercomputer at the University of Illinois. All production simulations were performed using OpenMM7.7.0.

eukaryotic counterparts. ^{1,12} As such, recent work has focused on elucidating the molecular mechanisms of post-translation modifications and its effect on human SLC6 transporters. ^{1,2} These studies include phosphorylation, ^{13–17} palmitoylation, ^{18,19} glycosylation, ^{20–24} and ubiquitination and its implications on transporter dynamics, stability, oligomerization, trafficking, and uptake activity.

The glycosylation of SLC6 transporters has been widely documented to affect transporter activity; 20-24 however, various mechanisms of how glycosylation mediates transporter function have been proposed for different SLC6 members. For example, glycosylation has been suggested to influence transporter stability in the membrane as demonstrated for the serotonin, dopamine, and norepinephrine transporters, 20,21,23 whereas in glycine and GABA transporters, glycosylation regulates membrane trafficking. 22,24 The removal of glycans did

not affect ligand binding or transport function for the serotonin and norepinephrine transporters; ^{20,23} however, mutagenesis of N-linked glycosylation sites in the dopamine and glycine 1 transporters resulted in reduced uptake rates. ^{21,22} Furthermore, the degree of glycosylation widely differs among expression organisms, tissues, and cell developmental periods. ^{26–28} As the mechanism of substrate transport is a cumulation of various functions, including expression, trafficking, binding, other post-translational modifications, and recognition with other proteins, the extent of glycosylation and its effect on conformational dynamics remain ambiguous.

With the surge in performance of graphical processing units and numerical algorithms, molecular dynamics (MD) simulations present a powerful approach to characterize post-translational modifications and its effect on protein structure and dynamics. Recent applications of atomistic simulations to

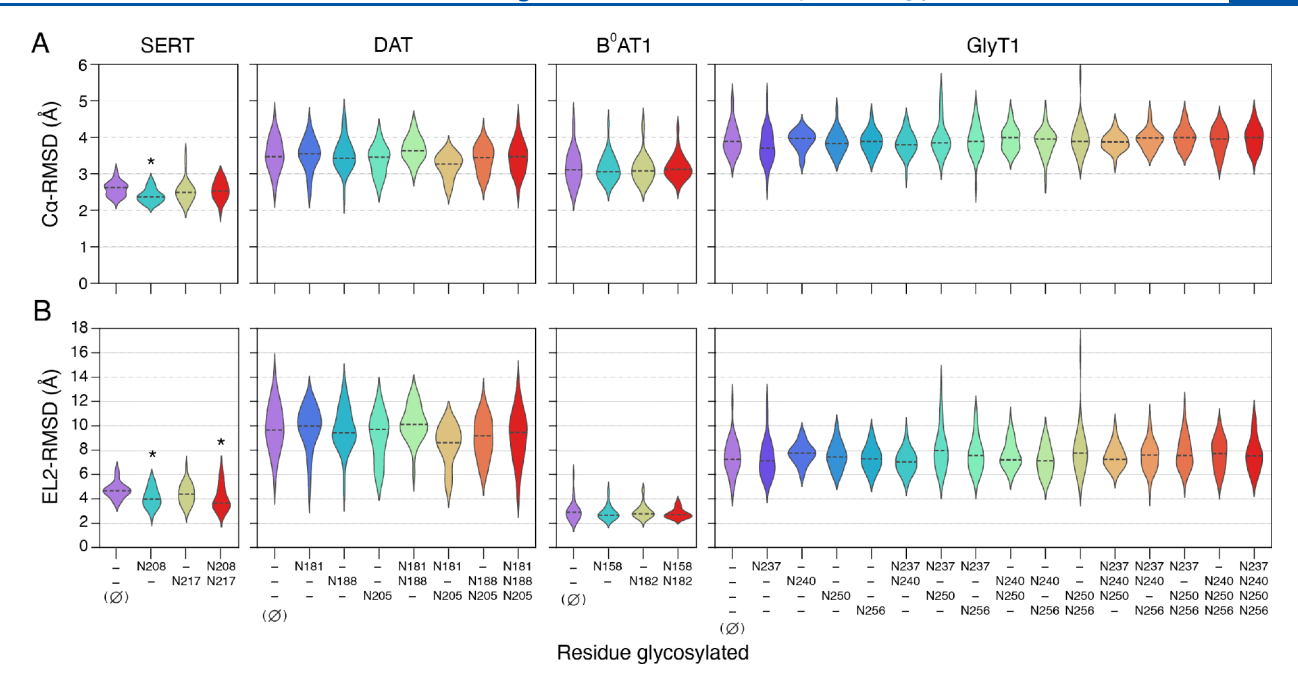


Figure 2. Glycosylation does not significantly affect the transporter structure. Distribution of the averaged (A) root-mean-square deviations (RMSDs) of all transporter $C\alpha$ atoms and (B) the RMSD of extracellular loop 2 (EL2) among the 1 μ s MD replicates for each respective system. The initial structure used for MD simulations was used as the respective reference for all calculations. The first 100 ns were excluded from RMSD calculations. Median values are indicated as dashed lines. An * indicates values significantly different (two-tailed Mann–Whitney U test, p < 0.05/n, Bonferroni corrected for n number of comparisons) from the respective deglycosylated transporter indicated as Ø. Mean values, standard error, median, and p-values are provided in Supporting Information Tables S2 and S3.

investigate post-translational modifications have identified how phosphorylation alters the hydrogen bonding network of the serotonin transporter, ¹⁴ glycosylation induces open conformations of the yeast disulfide isomerase, ²⁹ and nitration prevents ligand binding of a plant abscisic acid receptor. ³⁰ Moreover, MD simulations provide a technique to probe the structural dynamics in a label-free, fully atomistic approach, ideal for addressing the differences in experimental setup.

In this current work, we designed a MD study to systematically investigate the structural and dynamic consequences of N-linked glycosylation on SLC6/NSS transporters. While MD simulations have been employed to characterize the intrinsic dynamics of SLC6 transporters at full atomistic resolution, ^{31–34} the effects of glycosylation on dynamics have yet to be investigated computationally. To this end, we collected an aggregated simulation data set of $\sim 30 \ \mu s$ for each of the four studied human SLC6/NSS transporters (Figure 1A), the serotonin transporter (SERT, SLC6A4), the dopamine transporter (DAT, SLC6A3), the neutral amino acid transporter B⁰AT1 (SLC6A19), and the glycine transporter 1 (GlyT1, SLC6A9), to elucidate the role of glycans on structural stability and conformational dynamics. We first examined the effects of glycosylation on the four transporters with glycans attached to each glycosylation site of extracellular loop 2 (EL2) in a combinatorial fashion. In the second part of our study, we simulated the transporters with various degrees and complexity of oligoglycans to probe the influence of larger glycan molecules on the protein structure.

Our simulations suggest that glycosylation does not affect the overall transporter structure. However, the glycosylation of EL2 with a single glycan on each site consequently modulates its dynamics and surrounding regions but not in a uniform manner. Moreover, the presence of larger glycans further decreases EL2 loop dynamics. However, despite the decreased loop fluctuations, the distance distribution of the gating helices did not alter significantly. Overall, we conclude that glycosylation does not have a profound effect on dynamics associated with substrate transport and thus is likely more involved in cellular sensing and regulation in the cell.

RESULTS

Glycosylation Does Not Significantly Affect the Transporter Structure but Alters Loop Dynamics. The extracellular loop 2 of SLC6 transporters contains two to four N-linked glycosylation sites that follow the Asn-X-Ser/Thr amino acid sequence motif, where X is any residue except proline (Figure S1).³⁵ Previous biophysical characterization of NSS transporters has reveal the extracellular loops to be coupled with the substrate transport dynamics^{31,36,37} and substrate selectivity, 38,39 and as such, we hypothesized if the addition of bulky, hydrophobic glycans may affect the structure and dynamics of the transporter. We performed microsecond long MD simulations of four SLC6 transporters with an Nacetylglucosamine glycan modeled to each N-linked glycosylation site in a combinatorial fashion (Figure 1A and Table S1). Simulations were initiated from an outward-facing conformation with ions and the respective substrate bound in the orthosteric binding site and embedded in a multicomponent phospholipid bilayer (Figure 1B). A total of 29–30 MD replicates of 1 μ s long simulations were collected for each transporter and glycosylation state, resulting in an aggregated simulation data set of 949 μ s (Table S1).

The root-mean-square deviation (RMSD) with respect to the initial starting structure is presented in Figure 2. The simulated transporters remained stable across the 1 μ s with a C α RMSD of ~2.5–4 Å (Figure 2A). Furthermore, the simulations reveal that glycosylation does not significantly affect the overall transporter structure, with the exception of

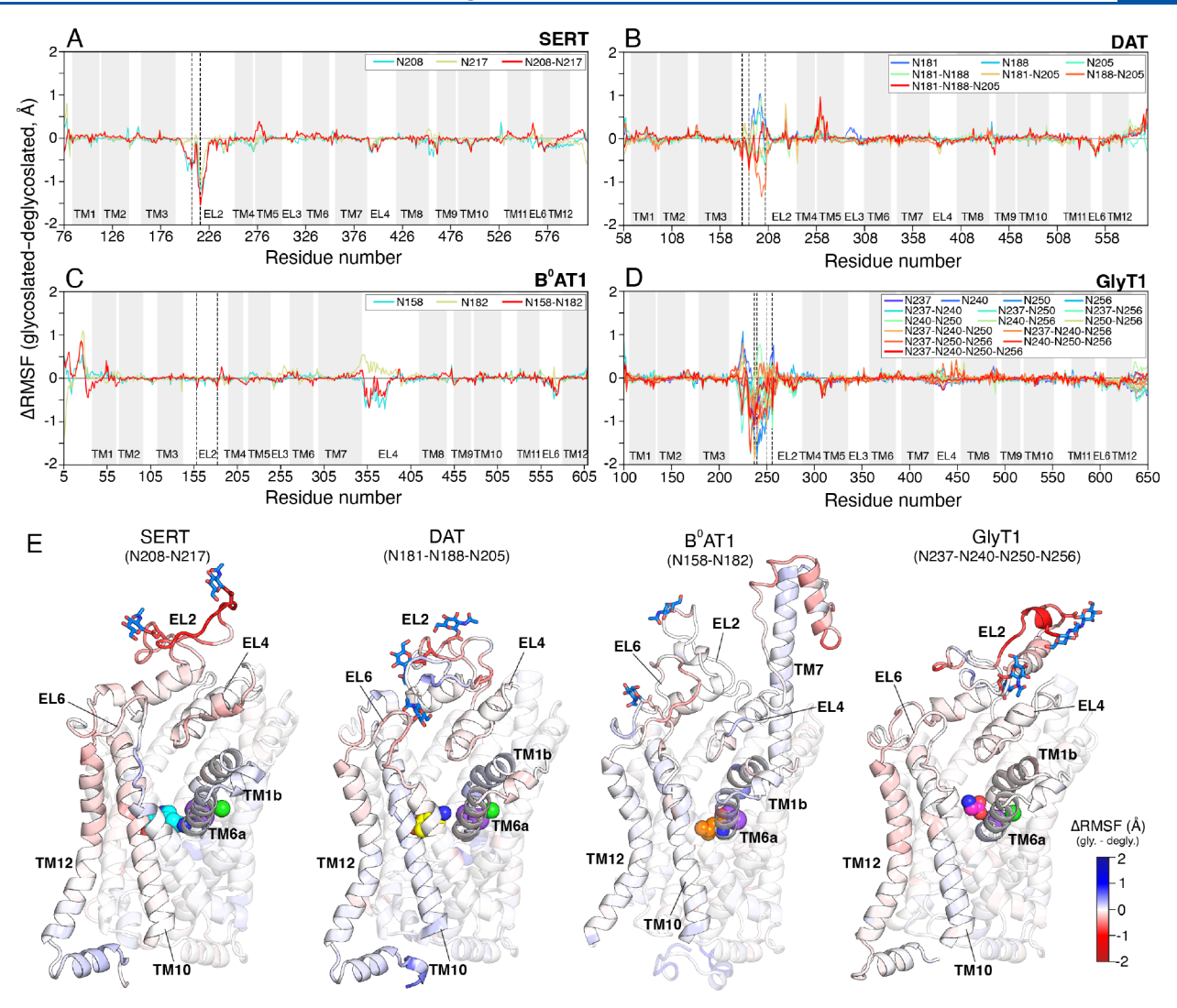


Figure 3. Difference RMSF plots of the glycosylated transporters. (A-D) The difference RMSF (Δ RMSF) in which the deglycosylated transporter was subtracted from the glycosylated transporter is plotted along the primary residue sequence. The initial structure used for MD simulations was used as the respective reference for RMSF calculations. Quantities are averaged from all 1 μ s MD replicates for each respective system. The glycosylated systems are plotted and colored according to Figure 2. Transmembrane helices are marked in gray regions along the residue numbers. N-linked glycosylation sites are marked by a black dashed line. (E) The difference RMSF (Δ RMSF) of the fully glycosylated transporter compared to the deglycosylated transporter plotted on the respective transporter structure.

SERT-N208 which exhibited a marginal decrease in RMSD as compared to the deglycosylated transporter (Figure 2A).

Despite structural and sequential conservation of the transporter core, the solvent-exposed loops vary in sequence and length among the SLC6 family. As such, the dynamics of the EL2 loop also varies between the studied transporters. Among the deglycosylated transporters, we observed that the shorter length EL2 in B⁰AT1 and SERT exhibited less structural deviations as compared to the longer length EL2 in DAT and GlyT1. However, when examining the effects of glycosylation on the EL2 structure, the simulations of glycosylated DAT, B⁰AT1, and GlyT1 were not observed to significantly differ from the respective deglycosylated transporters (Figure 2B). In contrast, only two glycosylated SERT systems, N208 and N208–N217, were found to have a significant decrease in EL2 RMSD (Figure 2B).

Figure 3 shows the difference per-residue RMSF with respect to the deglycosylated transporter for the four studied SLC6 transporters. The plots reveal that glycosylation alters the dynamics of EL2 in a differing manner among transporters

(Figure 3). In SERT simulations, glycosylation consistently decreases the fluctuations of EL2 as compared to the deglycosylated SERT (Figure 3A). However, the effects of glycosylation on EL2 dynamics vary and do not show a consistent trend among DAT and GlyT1 transporters (Figure 3B, D). In SERT and DAT, we observed the fully glycosylated transporter (SERT: N208-N217; DAT: N181-N188-N205) to increase the dynamics of the cytoplasmic base of TM5 (Figure 3A,B). Extensive literature supports the unwinding of the TM5 as a key structural rearrangement for propagating transition to the inward-facing state. 31,37,40,41 Furthermore, the number of glycosylated Asn residues did not appear to be correlated with effects on dynamics. Interestingly in B⁰AT1, glycosylation did not have a pronounced effect on EL2 dynamics but allosterically alters the displacements of the nearby EL4 (Figure 3C, E). The glycans were not observed to come into contact with EL4, but the cryo-EM complex reveals that EL4 and the extended TM7 play a role in trafficking and interfacing with the angiotensin-converting enzyme 2.42 EL4 of

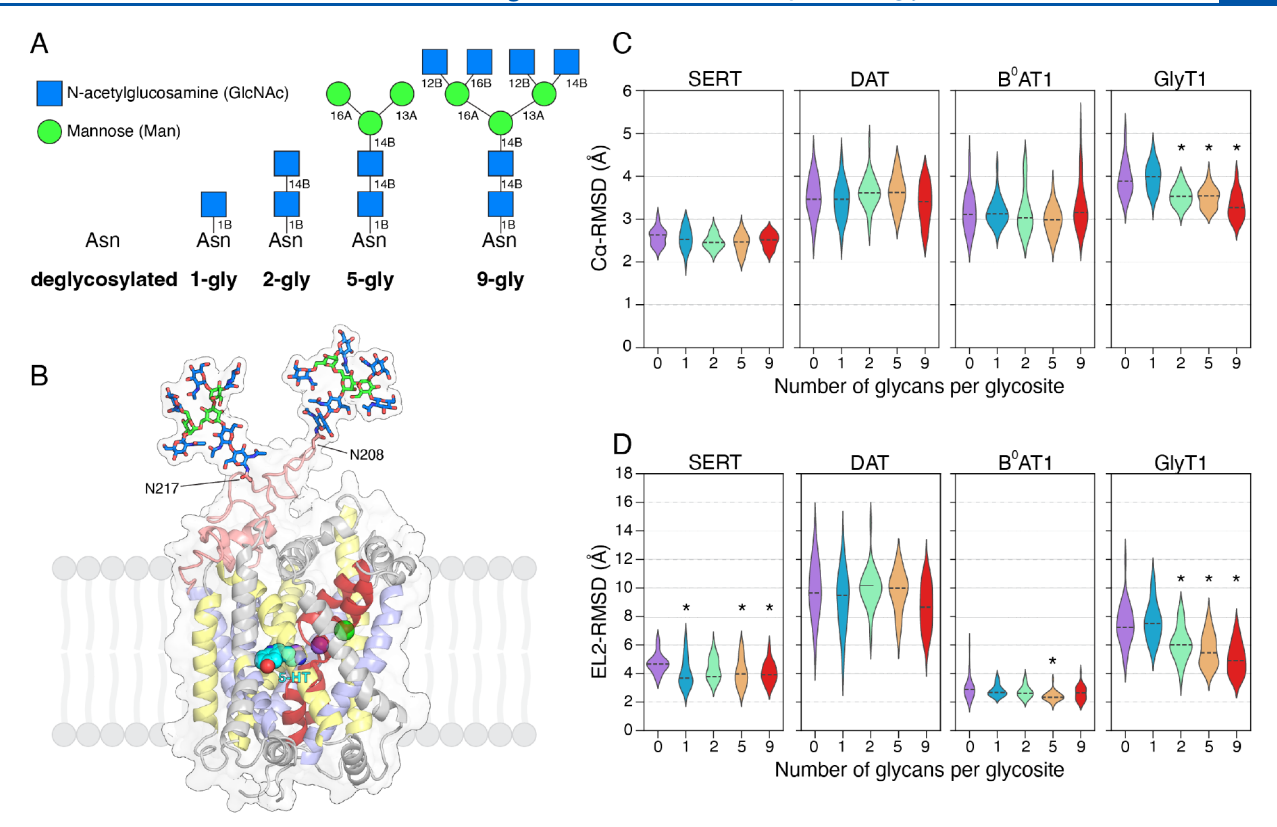


Figure 4. Structural effects of oligo-N-linked glycans. (A) The oligo-N-linked glycans modeled in this study. The oligoglycans were added to all glycosylation sites for each transporter and simulated under the same protocol as the single N-acetylglucosamine glycan simulations. (B) Representative structure of SERT and the 9-glycan group added to both glycosylation sites. Transmembrane helices and substrates are represented and colored according to Figure 1. (C, D) Structural measurements of the oligoglycan-transporter systems, similarly calculated as in Figure 2. The values of (C) Cα RMSD and (D) EL2 RMSD were averaged from the 1 μ s MD replicates for each respective system. The initial structure used for MD simulations was used as the respective reference for all calculations. The first 100 ns were excluded from RMSD calculations. Median values are indicated as dashed lines. An * indicates values significantly different (two-tailed Mann—Whitney U test, p < 0.05/n, Bonferroni corrected for n number of comparisons) from the respective deglycosylated transporter. Average values, standard error, median, and p-values are provided in the Supporting Information Tables S5 and S6.

B⁰AT1 contains a number of N-linked glycosylation sites, ⁴² but the effects of these sites were not investigated in this study.

Overall, though the difference in structural deviations is of a relatively small magnitude ($\sim 0.5-1.5$ Å), the effects Nglycosylation of EL2 do not consistently affect the structural dynamics within individual transporters nor across the sampled SLC6 family. Furthermore, principal component analysis of the $C\alpha$ fluctuations does not reveal discernible differences among the glycosylation patterns (Figure S2). From the simulations, we observed marginal differences (<1 Å) in the distance distributions of gating helices, thus suggesting that Nglycosylation does not have a profound effect on transport dynamics (Figure S3). Furthermore, glycosylation does not consistently affect the stability of the ligand bound in the orthosteric site, with the exception of SERT (Figure S4). The simulations of SERT and its glycosylated forms reveal that the RMSD of the serotonin, with respect to the initial bound pose, is decreased thus suggesting greater ligand stability upon glycosylation (Figure S4A). In all, the simulations reveal that the presence of hydrophobic glycans on a solvent-exposed domain of the transporter loop alters its local environment but does not propagate to the remainder of the transporter.

Oligo-N-Linked Glycosylation Further Stabilizes Loop Fluctuations. Though ubiquitous among eukaryotes, it is evident to note that the degrees of glycosylation and its regulatory role widely differ among species and cell types.²⁸

The previous body of literature has extensively explored the use of cell lines from a variety of organisms including, but not limited to, human (HEK-293), insect (Sf9), omnkey (COS), in figure (CHO). In the manner of the month of the previous cell types and developmental stages and thus further illuminate the complexity of glycosylation in the nervous system and throughout the body.

As it is not feasible to investigate all possible glycan and linkage patterns, nor has it been characterized in exact detail, we designed MD systems of the four SLC6 transporters in a pattern of increasing glycan moieties to serve as a representative and generic model of complex oligoglycans (Figure 4A). The complex glycans ranged from a linear 2 N-acetylglucosamine glycan to a branch oligoglycan containing 9 carbohydrates in total. For simulations of the oligoglycans, all Asn glycosylation sites on EL2 were modeled as the glycosylated form. Figure 4B shows a representative structure of the 9-glycan system for SERT. The glycosylated transporters were constructed in the same protocol as the single N-acetylglucosamine glycosylated transporter systems, and a total of 29–30 replicates were simulated for 1 μ s each, totaling an additional 359 μ s of aggregate data (Table S4).

Similar to simulations of the single N-acetylglucosamine glycosylated transporters, the simulations of the complex oligoglycans further suggest that N-glycosylation does not

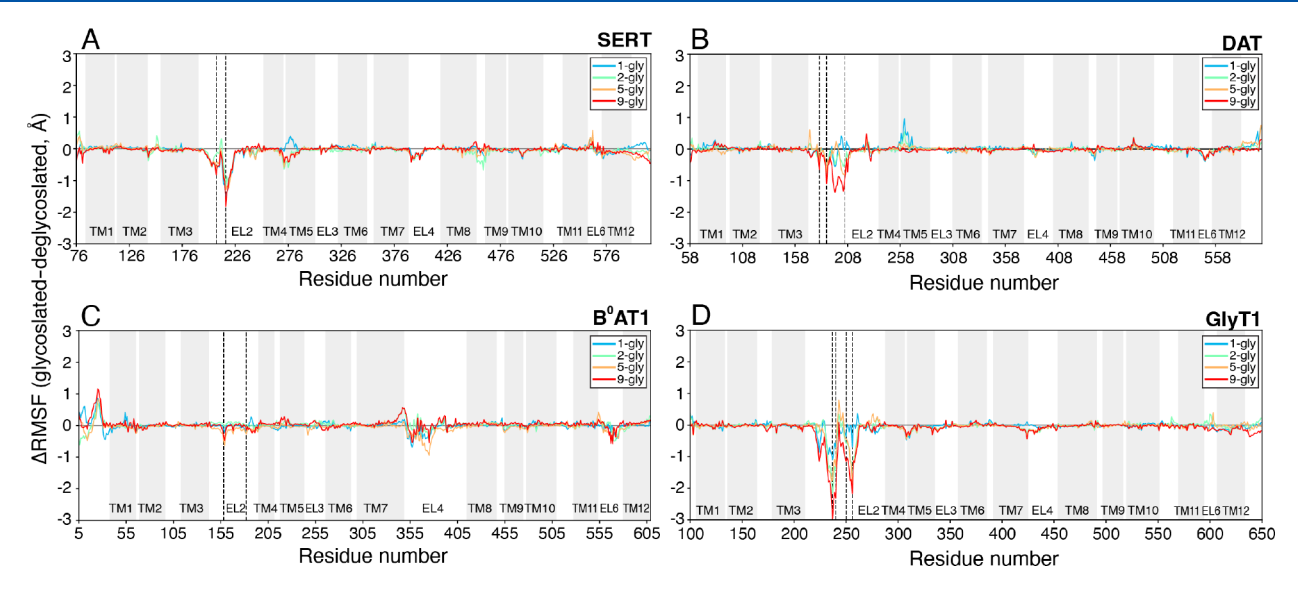


Figure 5. Difference RMSF plots of the oligo-glycosylated transporters. The difference RMSF (Δ RMSF) in which the deglycosylated (0-gly) transporter was subtracted from the glycosylated transporter is plotted along the primary residue sequence. The initial structure used for MD simulations was used as the respective reference for RMSF calculations. Quantities are averaged from all 1 μ s MD replicates for each respective system. MD systems with varying degrees of glycosylation are plotted and colored according to Figure 4. Transmembrane helices are marked in gray regions along the residue numbers. N-linked glycosylation sites are marked by a black dashed line.

uniformly affect SLC6 transporters. With regards to the overall transporter structure, when SERT, DAT, and B⁰AT1 were glycosylated to any degree, we did not observe differences among the sets of simulations (Figure 4C). When examining the structure and dynamics of EL2, the simulations for large simulated glycans (>5 glycans) reveal the RMSD of EL2 to be significantly lower compared to the deglycosylated transporters SERT and B⁰AT1 (Figure 4D). In SERT, the single Nacetylglucosamine added to both glycosylation sites, N208 and N217, was observed to decrease the EL2 RMSD (Figure 2B), but the presence of larger glycans did not significantly further influence the EL2 structure (Figure 4D). Most strikingly, increasing the number of glycans and complexity of linkages added to GlyT1 was correlated with a decrease in overall transporter and EL2 RMSD (Figure 4C, D). The 9-glycan GlyT1 was observed to have an EL2 RMSD of 5.027 ± 0.204 (mean \pm SEM) compared to the deglycosylated GlyT1 with an EL2 RMSD of 7.460 ± 0.261 .

The simulations further reveal that the dynamics of EL2 is reduced when glycosylated with complex oligoglycans, with the most significant differences observed with more glycans added per glycosylation site (Figure 4D). The RMSF plots of the oligo-glycosylated transporters illustrate that the fluctuations of EL2 are also altered compared to the deglycosylated transporter (Figure 5). The dynamics of EL2 on SERT and B⁰AT1 do not differ widely from the single N-acetylglucosamine glycosylated transporters (Figure 5A, C). However, more notably, the fluctuations for DAT and GlyT1 EL2 when glycosylated with the oligoglycans are generally diminished across all degrees of glycosylation (Figure 5B, D). Furthermore, the presence of the complex oligoglycans also did not consistently affect the motions of the gating helices (Figure S5) nor the stability of the bound ligand as similarly observed in the single N-acetylglucosamine transporter simulations (Figure S6).

The intrinsic dynamics of attached glycans has been previously identified to act as a hydrophobic barrier and shield the protein surface, disrupting protein—protein interactions.

Most notably, the use of MD simulations has characterized the extent of glycan shielding on key immunological targets including the SARS-CoV-2 spike protein⁴⁴ and viral envelop proteins. 45,46 We computed the solvent accessible surface area (SASA) to examine the effect of glycan shielding on the extracellular vestibule and surrounding regions. As expected, we observed the glycans to decrease the accessible surface area of residues on EL2 and the larger oligoglycans to progressively decrease the accessible surface area for surrounding EL2 residues (Figure S7). Furthermore, while the simulations did not reveal major differences in the accessible surface area SERT and GlyT1 with increasing complexity of glycosylation (Figure S8), we did find that glycans extend to decrease the accessibility of the DAT extracellular vestibule (Figure 6A). By overlaying the simulated conformational distribution of the glycan moieties, we observed the N205 glycans to extend beyond EL2 and shield the DAT extracellular vestibule (Figure 6A). In contrast, the glycans attached to SERT and GlyT1 do not extend to the extracellular vestibule (Figure S8). Interestingly in B⁰AT1, the glycans also do not directly shield the extracellular vestibule; however, the progressive addition of more glycans allosterically decreases the solvent accessibility of TM11, TM6a, and EL6 which make up an allosteric substrate binding site or S2 (Figure 6B). This conserved S2 site has been previously implicated to act as a selectivity filter for transporter substrates. 38,39 Taken together, these observations suggest that glycosylation may influence the transporter's ability to initially recognize and bind the substrate either through glycan shielding or allosterically modulating the S1 site.

DISCUSSION

The activity of SLC6 transporters is tightly controlled through intricate regulatory mechanisms. Consequently, dysregulation of transport activity is associated with various neurodegenerative, respiratory, and cardiovascular diseases. As these transporters are essential for maintaining cellular homeostasis, understanding the conformational heterogeneity and how post-

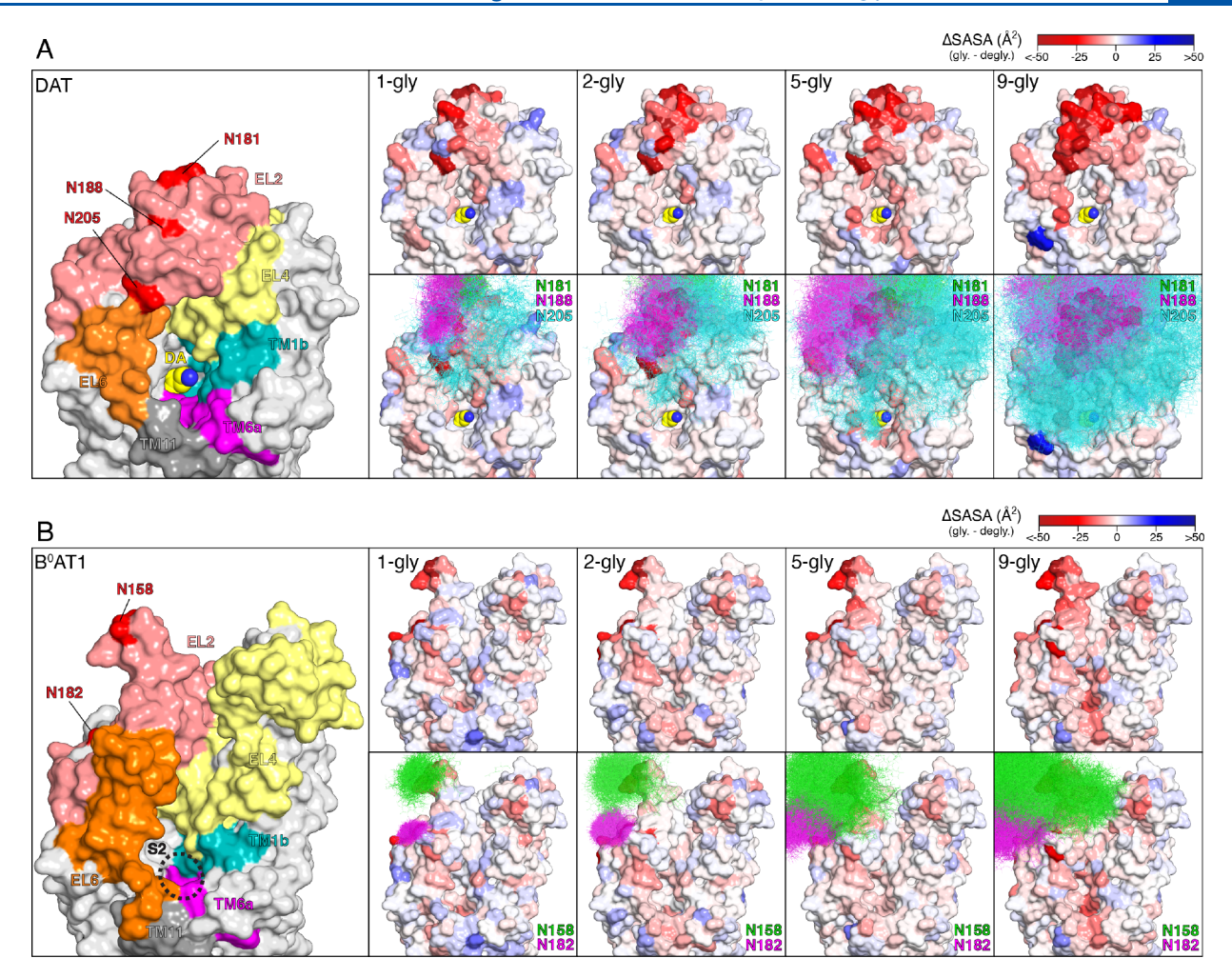


Figure 6. The effect of glycans on the solvent accessible surface area of the extracellular vestibule. The difference of the SASA of the oligoglycosylated transporter and the deglycosylated (0-gly) transporter is projected on the (A) DAT and (B) B^0AT1 three-dimensional structures. Regions colored in red indicate where the SASA is decreased in the glycosylation system as compared to the deglycosylated transporter. The extracellular vestibule is lined by TM1b (teal), TM6a (magenta), TM11 (dark gray), EL4 (yellow), and EL6 (orange) and is shown in the left-most panel for reference. The allosteric S2 site for B^0AT1 is circled in **B**. The positions of the glycans from the simulations are overlaid in the accompanying structures and colored according to its glycosylation site. The coordinates of the glycan molecules are extracted every 6 ns of each 1 μ s replicate. SASA projections for SERT and GlyT1 are shown in Figure S8.

translational modification alters the underlying dynamics is pivotal for designing effective therapeutic molecules.

SLC6 transporters possess 2-4 N-linked glycosylation sites on the solvent-exposed EL2. Hydrogen-deuterium exchange and molecular modeling have characterized the dynamics of EL2, and other extracellular loops, to be stabilized upon the structural rearrangements from outward-facing to inward-facing conformations. ^{31,36,37} We initially hypothesized the addition of glycans to the extracellular loops would alter the stability of the loops, thus potentially perturbing the conformational equilibria. However, while our simulations show that glycosylation does indeed stabilize EL2 loop dynamics, it does not influence overall transporter structure or conformational dynamics in the simulated time scales. We observed that the effects of glycosylation are small in quantity, and likely a larger sample size may more greatly illuminate these minute differences. Overall, we conclude that glycosylation does not have a significant effect on substrate transport dynamics and is more likely to be involved in other regulatory processes such as membrane stability and proper trafficking.

Glycosylation is an essential and universal post-translation modification for regulating protein function. The use of MD simulations enables a fully atomistic characterization of the structural and dynamic consequences of glycosylation 47,48 and other post-translational modifications. 14,49,50 Though glycosylation has been widely understood to affect SLC6 transporter stability and trafficking, 1,2 our simulations show that Nglycosylation minimally affects overall transporter dynamics but reduces the fluctuation of the extracellular loops. However, we did not observe glycosylation to consistently alter the SLC6 transporter structure which may further explain the differences in regulatory function previously characterized experimentally. Furthermore, previous simulations of glycoproteins further underline a lack of uniformity in regulating protein structure and dynamics^{47,51,52} and may suggest that the disruption of the local protein environment has a greater role in modulating dynamics and stability rather than the presence of glycans itself. Although, while the position of some glycans is more critical for regulating protein function,⁴⁴ the degree of the glycosylation may also have a profound effect on the dynamics as shown in the oligoglycan-transporter simulations

in this study. Thus, when investigating the structural dynamics of glycoproteins, we recommend to consider the potential effects of various glycans moieties, both in composition and arrangements, to obtain a comprehensive understanding of glycosylation.

METHODS

System Preparation. To investigate the effects of glycosylation on transporter dynamics and stability, we selected four human transporters from the SLC6/NSS family: the serotonin transporter (SERT), dopamine transporter (DAT), neutral amino-acid transporter B^0AT1 , and the glycine transporter 1 (GlyT1). These transporters have extensive structural and/or biochemical characterization of the effects of glycosylation. $^{5-7,20-22,42}$

We initiated all simulations from an outward-facing conformation with the transporter's respective substrates bound in the orthosteric pocket. The initial structures were obtained as follows: SERT, three-dimensional coordinates from the outward-facing crystal structure (PDB: 5IX6) with Na1, Na2, Cl⁻ bound, and serotonin (5-HT) modeled based on our previous MD simulation study;³¹ DAT, a homology model based on the outward-facing Drosophila melanogaster DAT crystal structure (PDB: 4XP1) with Na1, Na2, Cl⁻, and dopamine (DA) modeled based on the crystal structure; B⁰AT, three-dimensional coordinates from the outward-facing cryo-EM structure (PDB: 6M18) with Na1, Na2, and leucine based on the structural alignment with Leu-bound LeuT (PDB: 2A65); and GlyT1, a homology model based on the outwardfacing Drosophila melanogaster DAT crystal structure previously modeled by Zhang et al.⁵³ with Na1, Na2, Cl⁻ bound, and glycine bound based on the structural alignment with Glybound LeuT (PDB: 3F4J). The GlyT1 model did not initially contain extracellular loop 2 (EL2), and as such, we modeled the loop using the comparative modeling module of the ROBETTA web server.⁵⁴ The resulting EL2 model displayed alpha helical secondary structure elements at residues 235 to 239 and 243 to 252, which is further suggested by the IUPRED intrinsic disorder structure prediction web server.⁵⁵

The transporters were embedded in a 90 \times 90 Å² multicomponent phospholipid bilayer using the CHARMM-GUI web server. 56 For SERT, DAT, and GlyT1, the transporter was embedded in a 2:1 POPC:POPE symmetric lipid bilayer, loosely based on the neuronal plasma membrane composition.⁵⁷ As B⁰AT1 is expressed in the membrane of the small intestine,⁵⁸ we embedded the transporter in a 3:2:1 POPE:POPC:POPS membrane to mimic its native environment.⁵⁹ We note the exclusion of cholesterol molecules in the simulated membranes. While cholesterol is physiologically relevant in the human membrane environment, it has been extensively shown to sterically stabilize outward-facing conformations. 60,61 As such, we excluded cholesterol to prevent unintended inhibition of transporter dynamics. Nand C-termini were capped with acetyl and methyl amide groups, respectively. Titratable residues were modeled in accordance to pK_a calculations using PROPKA3.0.⁶² The systems were solvated with TIP3P water molecules and 150 mM NaCl. The mass of hydrogen atoms and connecting atoms was repartitioned accordingly to Hopkins et al.⁶³ For singleglycan simulations, an N-acetylglucosamine glycan was modeled to Asn glycosylation sites in a combinatorial fashion. For simulations of oligoglycans (2-gly, 5-gly, and 9-gly), the glycans were simultaneously modeled on all Asn glycosylation

sites. Individual details of constructed system are presented in Table S1 and S4.

Molecular Dynamics Simulations. Prior to production, the systems were minimized and equilibrated using the AMBER18 MD package employing the CHARMM36m force field. The CHARMM psf topology and coordinate files were converted to AMBER prmtop and rst7 files using the chamber module of the ParmEd package.⁶⁴ Each system was first subjected to an energy minimization protocol of 5,000 steps using the steepest descent method, followed by 45,000 minimization steps using the conjugate gradient method. The systems were then heated to 300 K for 5 ns in a constant particle, pressure, and temperature (NPT) ensemble, while the protein backbone, bound substrates, and glycans were restrained with a force constant of 5 kcal/mol-Å². The equilibrated snapshot was then converted to an OpenMM system parametrized with an OpenMM ForceField using the CHARMM36m force field.65

Production simulations were performed using the OpenMM 7.7.0 package⁶⁶ on either the Folding@Home distributing computing platform⁶⁷ or the University of Illinois National Center for Supercomputing Applications DELTA supercomputer. Langevin dynamics was performed using a Langevin integrator using an integration time step of 4 fs, temperature of 300 K, and collision rate of $\sqrt{2}$ ps⁻¹. The system pressure of 1 bar was maintained using the Monte Carlo Membrane Barostat with a surface tension of 200 bar-nm and update frequency of 100 steps. Nonbonded forces were calculated using the particle mesh Ewald method with a 12 Å cutoff distance. Simulations were performed using mixed numerical precision, periodic boundary conditions, and hydrogen mass repartitioning. 63 A total of 30 MD replicates for each system with different initial velocities were sent to Folding@Home users and simulated up to 1 μ s. Trajectories in which simulation data was not received from Folding@Home clients were not used for analysis. In all, a total of 29-30 1 µs long trajectories for each glycosylated system and transporter were collected and analyzed (Tables S1 and S4). Trajectory snapshots were saved every 100 ps during production simulations.

Trajectory Analysis. Trajectories were processed with inhouse scripts utilizing CPPTRAJ, pytraj, and MDTraj packages^{68,69} and visualized using Visual Molecular Dynamics (VMD)⁷⁰ and PyMOL. The root-mean-square deviations (RMSDs) of atomic positions were calculated on only $C\alpha$ atoms. The root-mean-square fluctuations (RMSFs) of each residue were calculated on all atoms and mass-averaged by residue. The initial structure used for production simulations was used as the reference for these calculations. A two-sided Whitney Mann U was performed to determine the significance of the RMSD between the glycosylated and the respective deglycosylated system. Principal component analysis of the C α atom fluctuations was performed using the scikit-learn Python library. $C\alpha$ atoms used for the center-of-mass calculations for the distance distribution of the gating helices are listed in Table S7. Plots were generated using the matplotlib and seaborn Python library.

DATA AND SOFTWARE AVAILABILITY

Molecular dynamics trajectories generated in this study are not publicly deposited as the data is over 1 TB in size. Data sets are available upon request and may require several business days to share. Once provided, we do not enforce any limitation for

how the data may be used once requested and shared. Analysis scripts are available at https://github.com/ShuklaGroup/SLC6_glycosylation.

ASSOCIATED CONTENT

Supporting Information

The Supporting Information is available free of charge at https://pubs.acs.org/doi/10.1021/acs.jcim.2c00940.

Multiple sequence alignment of EL2, distance distributions of gating helices, distribution of ligand RMSD with respect to the initial bound conformation, statistics of RMSD calculations, and overview of simulations performed for each study (PDF)

AUTHOR INFORMATION

Corresponding Author

Diwakar Shukla — Department of Chemical and Biomolecular Engineering, University of Illinois Urbana—Champaign, Urbana, Illinois 61801, United States; Center for Biophysics and Quantitative Biology, Department of Plant Biology, and Department of Bioengineering, University of Illinois Urbana—Champaign, Urbana, Illinois 61801, United States; orcid.org/0000-0003-4079-5381; Email: diwakar@illinois.edu

Author

Matthew C. Chan – Department of Chemical and Biomolecular Engineering, University of Illinois Urbana–Champaign, Urbana, Illinois 61801, United States; orcid.org/0000-0002-9826-1983

Complete contact information is available at: https://pubs.acs.org/10.1021/acs.jcim.2c00940

Author Contributions

M.C.C. designed and conducted the study. M.C.C. and D.S. analyzed the results. M.C.C. and D.S. prepared the manuscript.

Notes

The authors declare no competing financial interest.

ACKNOWLEDGMENTS

This work was supported by an NSF Early Career Award by NSF MCB 18-45606 to D.S. This research is also part of the Delta research computing project, which is supported by the National Science Foundation (award OCI 2005572), and the State of Illinois. Delta is a joint effort of the University of Illinois Urbana—Champaign and its National Center for Supercomputing Applications. The authors thank Folding@ Home donors for computational resources for this project. M.C.C. thanks Austin T. Weigle for insightful discussions and Nicole Chiang for technical assistance pertaining to this study.

REFERENCES

- (1) Pramod, A. B.; Foster, J.; Carvelli, L.; Henry, L. K. SLC6 transporters: Structure, function, regulation, disease association and therapeutics. *Mol. Aspects Med.* **2013**, *34*, 197–219.
- (2) Kristensen, A. S.; Andersen, J.; Jørgensen, T. N.; Sørensen, L.; Eriksen, J.; Loland, C. J.; Strømgaard, K.; Gether, U. SLC6 Neurotransmitter Transporters: Structure, Function, and Regulation. *Pharmacol. Rev.* **2011**, *63*, 585–640.
- (3) Yamashita, A.; Singh, S. K.; Kawate, T.; Jin, Y.; Gouaux, E. Crystal structure of a bacterial homologue of Na+/Cl-dependent neurotransmitter transporters. *Nature* **2005**, *437*, 215–223.

- (4) Forrest, L. R.; Rudnick, G. The Rocking Bundle: A Mechanism for Ion-Coupled Solute Flux by Symmetrical Transporters. *Physiology* **2009**, 24, 377–386.
- (5) Penmatsa, A.; Wang, K. H.; Gouaux, E. X-ray structure of dopamine transporter elucidates antidepressant mechanism. *Nature* **2013**, *503*, 85–90.
- (6) Coleman, J. A.; Green, E. M.; Gouaux, E. X-ray structures and mechanism of the human serotonin transporter. *Nature* **2016**, *532*, 334–339.
- (7) Shahsavar, A.; Stohler, P.; Bourenkov, G.; Zimmermann, I.; Siegrist, M.; Guba, W.; Pinard, E.; Sinning, S.; Seeger, M. A.; Schneider, T. R.; Dawson, R. J. P.; Nissen, P. Structural insights into the inhibition of glycine reuptake. *Nature* **2021**, *591*, *677*–*681*.
- (8) Motiwala, Z.; Aduri, N. G.; Shaye, H.; Han, G. W.; Lam, J. H.; Katritch, V.; Cherezov, V.; Gati, C. Structural basis of GABA reuptake inhibition. *Nature* **2022**, *606*, 820–826.
- (9) Quick, M.; Yano, H.; Goldberg, N. R.; Duan, L.; Beuming, T.; Shi, L.; Weinstein, H.; Javitch, J. A. State-dependent Conformations of the Translocation Pathway in the Tyrosine Transporter Tyt1, a Novel Neurotransmitter:Sodium Symporter from Fusobacterium nucleatum. *J. Biol. Chem.* **2006**, *281*, 26444–26454.
- (10) Androutsellis-Theotokis, A.; Goldberg, N. R.; Ueda, K.; Beppu, T.; Beckman, M. L.; Das, S.; Javitch, J. A.; Rudnick, G. Characterization of a Functional Bacterial Homologue of Sodium-dependent Neurotransmitter Transporters. *J. Biol. Chem.* **2003**, *278*, 12703—12709
- (11) Quick, M.; Javitch, J. A. Monitoring the function of membrane transport proteins in detergent-solubilized form. *Proc. Natl. Acad. Sci. U.S.A.* **2007**, *104*, 3603–3608.
- (12) Macek, B.; Forchhammer, K.; Hardouin, J.; Weber-Ban, E.; Grangeasse, C.; Mijakovic, I. Protein post-translational modifications in bacteria. *Nat. Rev. Microbiol.* **2019**, *17*, 651–664.
- (13) Quinlan, M. A.; Krout, D.; Katamish, R. M.; Robson, M. J.; Nettesheim, C.; Gresch, P. J.; Mash, D. C.; Henry, L. K.; Blakely, R. D. Human Serotonin Transporter Coding Variation Establishes Conformational Bias with Functional Consequences. *ACS Chem. Neurosci.* **2019**, *10*, 3249–3260.
- (14) Chan, M. C.; Procko, E.; Shukla, D. Structural Rearrangement of the Serotonin Transporter Intracellular Gate Induced by Thr276 Phosphorylation. ACS Chem. Neurosci. 2022, 13, 933–945.
- (15) Khoshbouei, H.; Sen, N.; Guptaroy, B.; Johnson, L.; Lund, D.; Gnegy, M. E.; Galli, A.; Javitch, J. A. N-Terminal Phosphorylation of the Dopamine Transporter Is Required for Amphetamine-Induced Efflux. *PLoS Biol.* **2004**, *2*, No. e78.
- (16) Vargas-Medrano, J.; Castrejon-Tellez, V.; Plenge, F.; Ramirez, I.; Miranda, M. PKC β -dependent phosphorylation of the glycine transporter 1. *Neurochem. Int.* **2011**, *59*, 1123–1132.
- (17) Cristóvão-Ferreira, S.; Vaz, S. H.; Ribeiro, J. A.; Sebastião, A. M. Adenosine A2A receptors enhance GABA transport into nerve terminals by restraining PKC inhibition of GAT-1. *J. Neurochem.* **2009**, *109*, 336–347.
- (18) Foster, J. D.; Vaughan, R. A. Palmitoylation Controls Dopamine Transporter Kinetics, Degradation, and Protein Kinase C-dependent Regulation. *J. Biol. Chem.* **2011**, 286, 5175–5186.
- (19) Zeppelin, T.; Pedersen, K. B.; Berglund, N. A.; Periole, X.; Schiøtt, B. Effect of palmitoylation on the dimer formation of the human dopamine transporter. *Sci. Rep.* **2021**, *11*, 4164.
- (20) Tate, C. G.; Blakely, R. D. The effect of N-linked glycosylation on activity of the Na(+)- and Cl(-)-dependent serotonin transporter expressed using recombinant baculovirus in insect cells. *J. Biol. Chem.* **1994**, 269, 26303–26310.
- (21) Li, L.-B.; Chen, N.; Ramamoorthy, S.; Chi, L.; Cui, X.-N.; Wang, L. C.; Reith, M. E. The Role of N-Glycosylation in Function and Surface Trafficking of the Human Dopamine Transporter. *J. Biol. Chem.* **2004**, 279, 21012–21020.
- (22) Olivares, L.; Aragón, C.; Giménez, C.; Zafra, F. The Role of N-Glycosylation in the Targeting and Activity of the GLYT1 Glycine Transporter. *J. Biol. Chem.* **1995**, *270*, 9437–9442.

- (23) Melikian, H. E.; Ramamoorthy, S.; Tate, C. G.; Blakely, R. D. Inability to N-glycosylate the human norepinephrine transporter reduces protein stability, surface trafficking, and transport activity but not ligand recognition. *Mol. Pharmacol.* **1996**, *50*, 266–276.
- (24) Cai, G.; Salonikidis, P. S.; Fei, J.; Schwarz, W.; Schülein, R.; Reutter, W.; Fan, H. The role of N-glycosylation in the stability, trafficking and GABA-uptake of GABA-transporter 1. *FEBS J.* **2005**, 272, 1625–1638.
- (25) Miranda, M.; Sorkin, A. Regulation of Receptors and Transporters by Ubiquitination: New Insights into Surprisingly Similar Mechanisms. *Mol. Interv.* **2007**, *7*, 157–167.
- (26) Lew, R.; Vaughan, R.; Simantov, R.; Wilson, A.; Kuhar, M. J. Dopamine transporters in the nucleus accumbens and the striatum have different apparent molecular weights. *Synapse* **1991**, *8*, 152–153.
- (27) Patel, A. P.; Cerruti, C.; Vaughan, R. A.; Kuhar, M. J. Developmentally regulated glycosylation of dopamine transporter. *Dev. Brain Res.* **1994**, *83*, 53–58.
- (28) Croset, A.; Delafosse, L.; Gaudry, J.-P.; Arod, C.; Glez, L.; Losberger, C.; Begue, D.; Krstanovic, A.; Robert, F.; Vilbois, F.; Chevalet, L.; Antonsson, B. Differences in the glycosylation of recombinant proteins expressed in HEK and CHO cells. *J. Biotechnol.* **2012**, *161*, 336–348.
- (29) Weiß, R. G.; Losfeld, M.-E.; Aebi, M.; Riniker, S. N-Glycosylation Enhances Conformational Flexibility of Protein Disulfide Isomerase Revealed by Microsecond Molecular Dynamics and Markov State Modeling. *J. Phys. Chem. B* **2021**, *125*, 9467–9479.
- (30) Shukla, S.; Zhao, C.; Shukla, D. Dewetting controls plant hormone perception and initiation of drought resistance signaling. *Structure* **2019**, *27*, 692–702.
- (31) Chan, M. C.; Selvam, B.; Young, H. J.; Procko, E.; Shukla, D. The substrate import mechanism of the human serotonin transporter. *Biophys. J.* **2022**, *121*, 715–730.
- (32) Cheng, M. H.; Bahar, I. Molecular Mechanism of Dopamine Transport by Human Dopamine Transporter. *Structure* **2015**, 23, 2171–2181.
- (33) Gradisch, R.; Szöllősi, D.; Niello, M.; Lazzarin, E.; Sitte, H. H.; Stockner, T. Occlusion of the human serotonin transporter is mediated by serotonin-induced conformational changes in the bundle domain. *J. Biol. Chem.* **2022**, *298*, 101613.
- (34) Grouleff, J.; Søndergaard, S.; Koldsø, H.; Schiøtt, B. Properties of an Inward-Facing State of LeuT: Conformational Stability and Substrate Release. *Biophys. J.* **2015**, *108*, 1390–1399.
- (35) Helenius, A.; Aebi, M. Roles of N-Linked Glycans in the Endoplasmic Reticulum. *Annu. Rev. Biochem.* **2004**, 73, 1019–1049.
- (36) Nielsen, A. K.; Möller, I. R.; Wang, Y.; Rasmussen, S. G. F.; Lindorff-Larsen, K.; Rand, K. D.; Loland, C. J. Substrate-induced conformational dynamics of the dopamine transporter. *Nat. Commun.* **2019**, *10*, 2714.
- (37) Merkle, P. S.; Gotfryd, K.; Cuendet, M. A.; Leth-Espensen, K. Z.; Gether, U.; Loland, C. J.; Rand, K. D. Substrate-modulated unwinding of transmembrane helices in the NSS transporter LeuT. *Sci. Adv.* **2018**, *4*, eaar6179.
- (38) Andersen, J.; Ringsted, K. B.; Bang-Andersen, B.; Strømgaard, K.; Kristensen, A. S. Binding site residues control inhibitor selectivity in the human norepinephrine transporter but not in the human dopamine transporter. *Sci. Rep.* **2015**, *5*, 15650.
- (39) Esendir, E.; Burtscher, V.; Coleman, J. A.; Zhu, R.; Gouaux, E.; Freissmuth, M.; Sandtner, W. Extracellular loops of the serotonin transporter act as a selectivity filter for drug binding. *J. Biol. Chem.* **2021**, 297, 100863.
- (40) Malinauskaite, L.; Quick, M.; Reinhard, L.; Lyons, J. A.; Yano, H.; Javitch, J. A.; Nissen, P. A mechanism for intracellular release of Na+ by neurotransmitter/sodium symporters. *Nat. Struct. Mol. Biol.* **2014**, *21*, 1006–1012.
- (41) Zhang, Y.-W.; Rudnick, G. The Cytoplasmic Substrate Permeation Pathway of Serotonin Transporter. *J. Biol. Chem.* **2006**, 281, 36213–36220.

- (42) Yan, R.; Zhang, Y.; Li, Y.; Xia, L.; Guo, Y.; Zhou, Q. Structural basis for the recognition of SARS-CoV-2 by full-length human ACE2. *Science* **2020**, *367*, 1444–1448.
- (43) Scott, H.; Panin, V. M. N-glycosylation in regulation of the nervous system. *Adv. Neurobiol.* **2014**, *9*, 367–394.
- (44) Casalino, L.; Gaieb, Z.; Goldsmith, J. A.; Hjorth, C. K.; Dommer, A. C.; Harbison, A. M.; Fogarty, C. A.; Barros, E. P.; Taylor, B. C.; McLellan, J. S.; Fadda, E.; Amaro, R. E. Beyond Shielding: The Roles of Glycans in the SARS-CoV-2 Spike Protein. *ACS Cent. Sci.* **2020**, *6*, 1722–1734.
- (45) Stewart-Jones, G. B.; Soto, C.; Lemmin, T.; Chuang, G.-Y.; Druz, A.; Kong, R.; Thomas, P. V.; Wagh, K.; Zhou, T.; Behrens, A.-J.; Bylund, T.; Choi, C. W.; Davison, J. R.; Georgiev, I. S.; Joyce, M. G.; Kwon, Y. D.; Pancera, M.; Taft, J.; Yang, Y.; Zhang, B.; Shivatare, S. S.; Shivatare, V. S.; Lee, C.-C. D.; Wu, C.-Y.; Bewley, C. A.; Burton, D. R.; Koff, W. C.; Connors, M.; Crispin, M.; Baxa, U.; Korber, B. T.; Wong, C.-H.; Mascola, J. R.; Kwong, P. D. Trimeric HIV-1-Env Structures Define Glycan Shields from Clades A, B, and G. Cell 2016, 165, 813—826.
- (46) Re, S.; Mizuguchi, K. Glycan Cluster Shielding and Antibody Epitopes on Lassa Virus Envelop Protein. *J. Phys. Chem. B* **2021**, *125*, 2089–2097.
- (47) Lee, H. S.; Qi, Y.; Im, W. Effects of N-glycosylation on protein conformation and dynamics: Protein Data Bank analysis and molecular dynamics simulation study. *Sci. Rep.* **2015**, *5*, 8926.
- (48) Shental-Bechor, D.; Levy, Y. Effect of glycosylation on protein folding: A close look at thermodynamic stabilization. *Proc. Natl. Acad. Sci. U.S.A.* **2008**, *105*, 8256–8261.
- (49) Kuzmanic, A.; Sutto, L.; Saladino, G.; Nebreda, A. R.; Gervasio, F. L.; Orozco, M. Changes in the free-energy landscape of p38 α MAP kinase through its canonical activation and binding events as studied by enhanced molecular dynamics simulations. *eLife* **2017**, *6*, No. e22175.
- (50) Moffett, A. S.; Bender, K. W.; Huber, S. C.; Shukla, D. Allosteric Control of a Plant Receptor Kinase through S-Glutathionylation. *Biophys. J.* **2017**, *113*, 2354–2363.
- (51) Price, J. L.; Shental-Bechor, D.; Dhar, A.; Turner, M. J.; Powers, E. T.; Gruebele, M.; Levy, Y.; Kelly, J. W. Context-Dependent Effects of Asparagine Glycosylation on Pin WW Folding Kinetics and Thermodynamics. *J. Am. Chem. Soc.* **2010**, *132*, 15359–15367.
- (52) Fonseca-Maldonado, R.; Vieira, D. S.; Alponti, J. S.; Bonneil, E.; Thibault, P.; Ward, R. J. Engineering the Pattern of Protein Glycosylation Modulates the Thermostability of a GH11 Xylanase. *J. Biol. Chem.* **2013**, 288, 25522–25534.
- (53) Zhang, Y.-W.; Uchendu, S.; Leone, V.; Bradshaw, R. T.; Sangwa, N.; Forrest, L. R.; Rudnick, G. Chloride-dependent conformational changes in the GlyT1 glycine transporter. *Proc. Natl. Acad. Sci. U.S.A.* **2021**, *118*, No. e2017431118.
- (54) Kim, D. E.; Chivian, D.; Baker, D. Protein structure prediction and analysis using the Robetta server. *Nucleic Acids Res.* **2004**, *32*, W526–W531.
- (55) Mészáros, B.; Erdős, G.; Dosztányi, Z. IUPred2A: context-dependent prediction of protein disorder as a function of redox state and protein binding. *Nucleic Acids Res.* **2018**, *46*, W329–W337.
- (56) Jo, S.; Kim, T.; Iyer, V. G.; Im, W. CHARMM-GUI: A webbased graphical user interface for CHARMM. *J. Comput. Chem.* **2008**, 29, 1859–1865.
- (57) Wilson, K. A.; MacDermott-Opeskin, H. I.; Riley, E.; Lin, Y.; O'Mara, M. L. Understanding the Link between Lipid Diversity and the Biophysical Properties of the Neuronal Plasma Membrane. *Biochemistry* **2020**, *59*, 3010–3018.
- (58) Vuille-dit-Bille, R. N.; Camargo, S. M.; Emmenegger, L.; Sasse, T.; Kummer, E.; Jando, J.; Hamie, Q. M.; Meier, C. F.; Hunziker, S.; Forras-Kaufmann, Z.; Kuyumcu, S.; Fox, M.; Schwizer, W.; Fried, M.; Lindenmeyer, M.; Götze, O.; Verrey, F. Human intestine luminal ACE2 and amino acid transporter expression increased by ACE-inhibitors. *Amino Acids* **2015**, *47*, 693–705.

- (59) Forstner, G. G.; Tanaka, K.; Isselbacher, K. J. Lipid composition of the isolated rat intestinal microvillus membrane. *Biochem. J.* **1968**, *109*, 51–59.
- (60) Laursen, L.; Severinsen, K.; Kristensen, K. B.; Periole, X.; Overby, M.; Müller, H. K.; Schiøtt, B.; Sinning, S. Cholesterol binding to a conserved site modulates the conformation, pharmacology, and transport kinetics of the human serotonin transporter. *J. Biol. Chem.* **2018**, 293, 3510–3523.
- (61) Zeppelin, T.; Ladefoged, L. K.; Sinning, S.; Periole, X.; Schiøtt, B. A direct interaction of cholesterol with the dopamine transporter prevents its out-to-inward transition. *PLOS Comput. Biol.* **2018**, *14*, No. e1005907.
- (62) Olsson, M. H. M.; Søndergaard, C. R.; Rostkowski, M.; Jensen, J. H. PROPKA3: Consistent Treatment of Internal and Surface Residues in Empirical pKa Predictions. *J. Chem. Theory Comput.* **2011**, 7, 525–537.
- (63) Hopkins, C. W.; Le Grand, S.; Walker, R. C.; Roitberg, A. E. Long-time-step molecular dynamics through hydrogen mass repartitioning. *J. Chem. Theory Comput.* **2015**, *11*, 1864–1874.
- (64) Shirts, M. R.; Klein, C.; Swails, J. M.; Yin, J.; Gilson, M. K.; Mobley, D. L.; Case, D. A.; Zhong, E. D. Lessons learned from comparing molecular dynamics engines on the SAMPL5 dataset. *J. Comput. Aided Mol. Des.* **2017**, *31*, 147–161.
- (65) Huang, J.; Rauscher, S.; Nawrocki, G.; Ran, T.; Feig, M.; de Groot, B. L.; Grubmüller, H.; MacKerell, A. D. CHARMM36m: an improved force field for folded and intrinsically disordered proteins. *Nat. Methods* **2017**, *14*, 71–73.
- (66) Eastman, P.; Swails, J.; Chodera, J. D.; McGibbon, R. T.; Zhao, Y.; Beauchamp, K. A.; Wang, L.-P.; Simmonett, A. C.; Harrigan, M. P.; Stern, C. D.; Wiewiora, R. P.; Brooks, B. R.; Pande, V. S. OpenMM 7: Rapid development of high performance algorithms for molecular dynamics. *PLOS Comput. Biol.* **2017**, *13*, No. e1005659.
- (67) Shirts, M.; Pande, V. S. Screen savers of the world unite. *Science* **2000**, 290, 1903–1904.
- (68) Roe, D. R.; Cheatham, T. E. PTRAJ and CPPTRAJ: Software for Processing and Analysis of Molecular Dynamics Trajectory Data. *J. Chem. Theory Comput.* **2013**, *9*, 3084–3095.
- (69) McGibbon, R. T.; Beauchamp, K. A.; Harrigan, M. P.; Klein, C.; Swails, J. M.; Hernández, C. X.; Schwantes, C. R.; Wang, L.-P.; Lane, T. J.; Pande, V. S. MDTraj: A Modern Open Library for the Analysis of Molecular Dynamics Trajectories. *Biophys. J.* **2015**, *109*, 1528–1532.
- (70) Humphrey, W.; Dalke, A.; Schulten, K. VMD: Visual molecular dynamics. J. Mol. Graph. 1996, 14, 33–38.